© 2019. Published by The Company of Biologists Ltd | Journal of Cell Science (2019) 132, jcs221952. doi:10.1242/jcs.221952

SHORT REPORT

Synaptotagmin 5 regulates Ca^{2+}-dependent Weibel–Palade body exocytosis in human endothelial cells

Camille Lenzi[1], Jennifer Stevens[2,*], Daniel Osborn[1], Matthew J. Hannah[3], Ruben Bierings[4,‡] and Tom Carter[1,§]

ABSTRACT

Elevations of intracellular free Ca^{2+} concentration ($[Ca^{2+}]_i$) are a potent trigger for Weibel–Palade body (WPB) exocytosis and secretion of von Willebrand factor (VWF) from endothelial cells; however, the identity of WPB-associated Ca^{2+}-sensors involved in transducing acute increases in $[Ca^{2+}]_i$ into granule exocytosis remains unknown. Here, we show that synaptotagmin 5 (SYT5) is expressed in human umbilical vein endothelial cells (HUVECs) and is recruited to WPBs to regulate Ca^{2+}-driven WPB exocytosis. Western blot analysis of HUVECs identified SYT5 protein, and exogenously expressed SYT5–mEGFP localised almost exclusively to WPBs. shRNA-mediated knockdown of endogenous SYT5 (shSYT5) reduced the rate and extent of histamine-evoked WPB exocytosis and reduced secretion of the WPB cargo VWF-propeptide (VWFpp). The shSYT5-mediated reduction in histamine-evoked WPB exocytosis was prevented by expression of shRNA-resistant SYT5–mCherry. Overexpression of SYT5–EGFP increased the rate and extent of histamine-evoked WPB exocytosis, and increased secretion of VWFpp. Expression of a Ca^{2+}-binding defective SYT5 mutant (SYT5-Asp197Ser–EGFP) mimicked depletion of endogenous SYT5. We identify SYT5 as a WPB-associated Ca^{2+} sensor regulating Ca^{2+}-dependent secretion of stored mediators from vascular endothelial cells.

KEY WORDS: Endothelial, Synaptotagmin, Weibel–Palade body, Exocytosis, Ca^{2+}, Secretion

INTRODUCTION

Endothelial cells store von Willebrand factor (VWF) and a complex mixture of inflammatory mediators, vasoactive peptides and regulators of tissue growth in special secretory granules called Weibel–Palade bodies (WPBs) (Knipe et al., 2010; Schillemans et al., 2018a; van Breevoort et al., 2012). WPB cargo molecules act together at sites of vessel injury to reduce blood loss, control infection and aid in tissue repair, but have also been implicated in various disease states (see later). WPBs undergo different modes of exocytosis resulting in rapid (subsecond) cargo release (Babich et al., 2008; Conte et al., 2015), selective cargo secretion (Babich et al., 2008; Nightingale et al., 2018), and compound or cumulative exocytosis (Kiskin et al., 2014; Valentijn et al., 2011), as well as slower forms of cargo release (2–10 s) requiring post-fusion recruitment of actomyosin to the WPB (Nightingale et al., 2011). Physiological and pathological mediators can trigger VWF secretion through several intracellular signalling pathways (Huang et al., 2012; Lowenstein et al., 2005; Schillemans et al., 2018a); however, sustained elevations of intracellular free Ca^{2+} concentration ($[Ca^{2+}]_i$) constitute a particularly potent trigger (Birch et al., 1994; Zupančič et al., 2002). Surprisingly, little is known about how increases in $[Ca^{2+}]_i$ are sensed and transduced into WPB exocytosis. Early studies identified a role for calmodulin (CaM) in Ca^{2+}-driven VWF secretion (Birch et al., 1992). Ca^{2+}-CaM binds the guanine nucleotide exchange factor RalGDS, which activates the small GTPase RalA (Rondaij et al., 2008). RalA binds components of the exocyst complex, which is involved in vesicle–plasma membrane docking, but also stimulates phospholipase D1 (PLD1) activity through activation of ADP-ribosylation factor 6 (Arf6) (Vitale et al., 2005). The latter is important for Ca^{2+}-driven VWF secretion (Disse et al., 2009), and together these processes provide a mechanism to generate domains at the plasma membrane that directly, or through recruitment of adapter proteins, promote WPB docking and fusion. Annexin A2 (AnxA2) in complex with the Ca^{2+}-binding protein S100A10 may represent one such adapter complex (Brandherm et al., 2013; Chehab et al., 2017; Gerke, 2016). Cytosolic AnxA2 is recruited to the plasma membrane by acidic phospholipids, such as phosphatidic acid, where it promotes further phospholipid clustering (Gerke, 2016). Importantly, S100A10 can bind the WPB-Rab27A-associated effector Munc13-4 (also known as UNC13D) (Chehab et al., 2017) providing a molecular scaffold linking the WPB to the plasma membrane. WPBs may also engage the plasma membrane through a Rab27A–Slp4a–syntaxin binding protein 1 (STXBP1) complex (Bierings et al., 2012; van Breevoort et al., 2014). Once close to the plasma membrane, WPB fusion is driven by SNARE proteins (see Schillemans et al., 2018b; van Breevoort et al., 2014 and references therein) and is, almost universally, regulated by one or more vesicle-associated Ca^{2+} sensors (Südhof, 2014). The nature of the WPB-associated Ca^{2+}-sensors that regulate WPB fusion remain unknown. The best characterised family of vesicle-associated Ca^{2+}-sensors are the synaptotagmins (SYTs) (Chapman, 2008; Südhof, 2014). There are 17 mammalian SYT isoforms (Craxton, 2010) and all share a common basic structure consisting of a short highly variable N-terminal region, a transmembrane domain, a linker region, and two C-terminal C2A and C2B domains that mediate Ca^{2+}-dependent binding to phospholipids (Pang and Südhof, 2010). The properties of Ca^{2+}-dependent phospholipid binding/dissociation and capacity to drive membrane fusion vary between the different SYT family members (Bai et al., 2004; Davis et al., 1999; Hui et al., 2005), and studies indicate that multiple SYT isoforms (both Ca^{2+}-dependent and

[1]Molecular and Clinical Sciences Research Institute, St George's, University of London, London SW18 ORE, UK. [2]MRC National Institute for Medical Research, London NW7 1AA, UK. [3]Microbiology Services Colindale, Public Health England, London, NW9 5EQ, UK. [4]Plasma Proteins, Sanquin Research and Landsteiner Laboratory, Academic Medical Centre, University of Amsterdam, 1006 AD Amsterdam, PO Box 9190, The Netherlands.
*Present address: Kings College London, Strand, London WC2R 2LS, UK.
‡Present address: Hematology, Erasmus University Medical Center, 3000 CA Rotterdam, PO Box 2040, The Netherlands

§Author for correspondence (tcarter@sgul.ac.uk)

R.B., 0000-0002-1205-9689; T.C., 0000-0002-6248-7278

Received 23 July 2018; Accepted 9 January 2019

Journal of Cell Science (2019) 132, jcs221952. doi:10.1242/jcs.221952

-independent; von Poser et al., 1997) contribute to fine tuning vesicle fusion kinetics to the specific needs of the cell (Luo and Sudhof, 2017; Rao et al., 2017; Robinson et al., 2002). Here, we show that SYT5 is expressed in human umbilical vein endothelial cells (HUVECs) and is recruited to WPBs, where it regulates Ca^{2+}-driven WPB exocytosis.

RESULTS AND DISCUSSION

SYT5 is expressed in HUVECs and localises to WPBs

Western blot analysis showed SYT5 is expressed in HUVECs (Fig. 1A). Our commercial antibody to SYT5 did not recognise SYT5 in immunocytochemistry experiments, so instead we expressed SYT5–mEGFP and analysed the subcellular localisation by counter-staining with antibodies to different subcellular compartments. SYT5–mEGFP colocalised almost exclusively with WPBs (Fig. 1B; Fig. S1) and was detected on perinuclear TGN46-positive WPBs, indicating that SYT5 is incorporated into the WPB during its formation (Fig. S1A). Overlap analysis of EGFP (green) and WPB-VWF (red) signals in dual-labelled images gave Manders' colocalisation coefficients M1 (green overlap with red) and M2 (red overlap with green) of 0.998±0.0007 (s.e.m.) and 0.838±0.025, respectively (n=10 cells). The molecular basis for SYT5 trafficking to secretory granules, remains unclear, although studies of other SYTs (e.g. SYT1 and SYT7) show that the N-terminal regions and palmitoylation of cysteine residues within the linker between the transmembrane and C2A domains play important roles in directing these SYTs to their target membranes (Han et al., 2004; Kang et al., 2004). Because SYT1 is reported to localise to pseudo-WPBs in AtT20 cells (Blagoveshchenskaya et al., 2002), we also analysed this SYT in HUVECs. Although SYT1 protein was detected (Fig. S2A), SYT1–EGFP localised to the plasma membrane and not WPBs (Fig. S2B,C). shRNA-mediated depletion of endogenous SYT1 mRNA had no significant effect on VWF-propeptide (VWFpp) secretion (Fig. S2D) indicating that SYT1 does not regulate WPB exocytosis. Having established that SYT5 can be recruited to WPBs, we next determined whether it might play a role in regulating Ca^{2+}-dependent hormone-evoked WPB exocytosis.

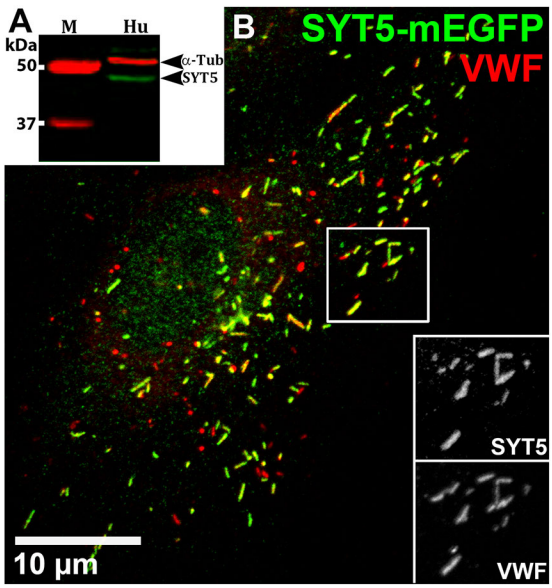

Fig. 1. SYT5 is expressed in HUVECs and recruited to WPBs. (A) Representative western blot of HUVECs (Hu) lysate probed with rabbit anti-SYT5 primary antibody (Abcam, ab116452, 1:200). Marker sizes (M) are indicated. α-tubulin was used as a loading control. The strong band at ∼48 kDa represents SYT5 protein, confirmed by depletion after shSYT5 treatment (Fig. 2). (B) Confocal fluorescence image of a HUVEC 48 h after Nucleofection™ with SYT5–mEGFP. Cells were immunolabelled with antibodies to GFP (sheep; green) and VWF (rabbit; red). Scale bar: 10 µm. Inset panels (greyscale) here and below are from regions indicated by white boxes. Manders' colocalisation coefficients for the fractional overlap of EGFP signal with that of the WPB–VWF signal (Manders' coefficient M1) was 0.998±0.0007 (s.e.m.) and for WPB–VWF signal overlapping the EGFP signal (Manders' coefficient M2) was 0.838±0.025 (n=10 cells).

Depletion of SYT5 modulates histamine-evoked VWFpp secretion and WPB exocytosis

We depleted endogenous SYT5 by means of shRNA (shSYT5) using a lentiviral vector with a puromycin selection cassette that allowed dual expression and selection of cells expressing both the shSYT5 (or shcontrol; shCTRL) and VWFpp–EGFP, enabling fluorescent labelling of WPBs in transduced cells. Transduced cells were directly monitored for fluorescent WPB exocytosis evoked by the physiological Ca^{2+}-dependent secretagogue histamine (Erent et al., 2007; Hamilton and Sims, 1987; Lorenzi et al., 2008). shSYT5 treatment reduced the level of SYT5 mRNA by 73% (Fig. 2A) and SYT5 protein by >65% (Fig. 2B). Comparison of changes in $[Ca^{2+}]_i$ during histamine (100 µM) stimulation of Fura-2-loaded HUVECs in shCTRL- or shSYT5-transduced cells showed no effect of shSYT5 treatment (Fig. 2C, upper panel); however in the same experiments, the kinetics and extent of fluorescent WPB exocytosis was significantly altered in shSYT5 transduced cells (Fig. 2C, lower panel). There was a significant reduction in the mean maximal rate of WPB exocytosis in response to histamine (shCTRL, 2.2±0.4 WPBs/second, n=35 cells; shSYT5, 1.3±0.1 WPBs/second, mean±s.e.m., n=46 cells, P=0.043, t-test) and a reduction in the fraction of fluorescent WPBs that underwent exocytosis (shCTRL, black trace, 30.8±2.1%, 527 fusion events, n=35 cells; shSYT5, grey trace,18.1±1.3%, 507 fusion events, mean±s.e.m., n=46 cells, P<0.0001, t-test). SYT5 depletion had no effect on WPB movements close to the plasma membrane or on the fraction of WPBs showing restricted movements (Fig. S3A). Overexpression of SYT5–mCherry containing seven silent mutations in the region targeted by shSYT5 [SYT5–mCherry (7sm)], labelled WPBs and prevented inhibition of WPB exocytosis in shSYT5-treated cells (Fig. S4). Consistent with direct analysis of WPB exocytosis, we found that histamine-evoked VWFpp secretion was reduced in shSYT5-treated cells (Fig. 2D). At 100 µM histamine, the reduction in secretion was ∼40% compared to shCTRL, similar to the ∼40% reduction in WPB exocytosis observed directly by live-cell imaging.

SYT5 overexpression increases histamine-evoked VWFpp secretion and WPB exocytosis

We next examined the effect of SYT5–mEGFP overexpression on WPB exocytosis and VWFpp secretion. Overexpressed SYT5–mEGFP labels WPBs exclusively, allowing us to directly visualise the organelles and their exocytosis by monitoring changes in WPB morphology and the abrupt loss of WPB SYT5–EGFP fluorescence, as described previously for other WPB membrane proteins (Knipe et al., 2010). SYT5–mEGFP overexpression was compared to data from VWFpp–EGFP-expressing HUVECs as a control and the data (Fig. 3) is presented in the same way as in Fig. 2C. Histamine evoked identical increases in $[Ca^{2+}]_i$ in HUVECs expressing SYT5–EGFP (grey) and the control

Journal of Cell Science (2019) 132, jcs221952. doi:10.1242/jcs.221952

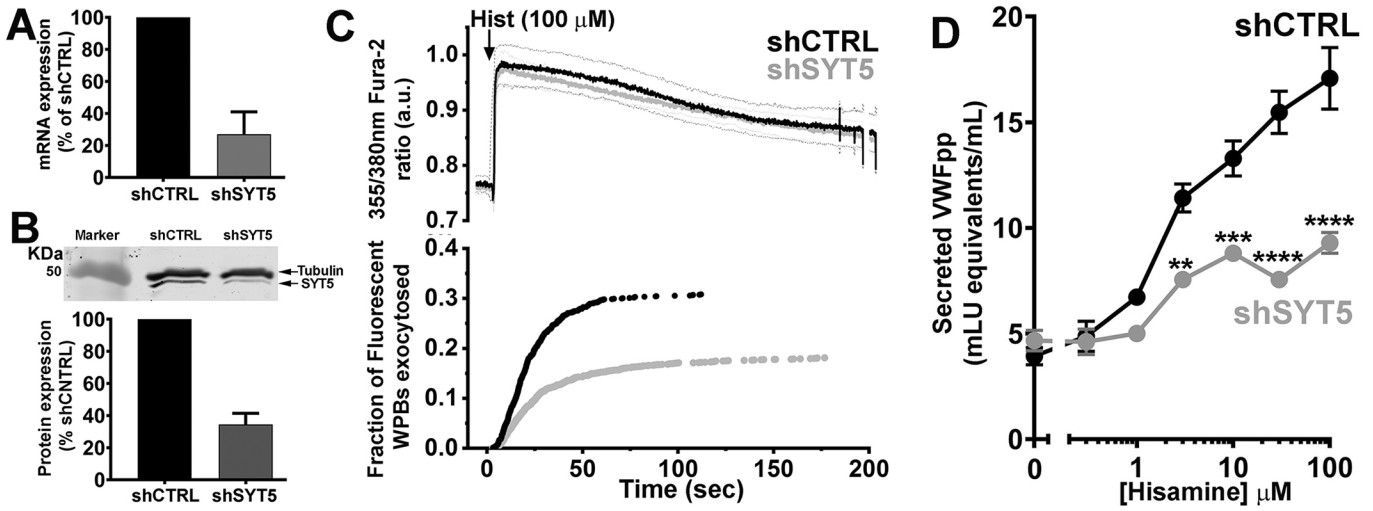

Fig. 2. SYT5 depletion reduces WPB exocytosis and VWFpp secretion. (A) Quantification of shRNA-mediated SYT mRNA depletion after lentiviral transduction. Data is normalised to shCTRL (mean±s.e.m. of four independent experiments). (B) Top, western blot showing SYT5 depletion after shRNA transduction. Bottom, quantification of SYT5 depletion (mean±s.e.m of four independent experiments). SYT5 was detected using a rabbit SYT5 primary antibody (Abcam, ab116452, 1:200); α-tubulin was used as loading control. (C) The top panel shows the mean 355 nm/380 nm Fura-2 fluorescence ratio recorded in shCTRL (black, *n*=12 cells) or shSYT5 (grey, *n*=12 cells)-treated HUVECs expressing VWFpp–EGFP and stimulated with histamine (100 µM, arrow). Thin dashed lines show the ±95% confidence limits for the mean fluorescence ratios (black, shCTRL; grey, shSYT5). The lower panel shows the cumulative plot of histamine-evoked WPB fusion times scaled to the mean fraction of WPBs that underwent exocytosis. (D) The level of histamine (0.3–100 µM)-evoked VWFpp secretion from HUVECs following lentiviral transduction with shCTRL (black) or shSYT5 (grey). Data are mean±s.e.m of four independent experiments, each carried out in triplicate. **P*≤0.05, ***P*≤0.01, ****P*≤0.001, *****P*≤0.0001, *t*-test.

VWFpp–EGFP (black) (Fig. 3A, upper panels). However, in SYT5–mEGFP-expressing cells, there was a significant increase in the mean maximal rate of WPB exocytosis from 2.1±0.31 WPBs/second (VWFpp–EGFP; *n*=30) to 5.9±2.4 WPBs/second (SYT5–EGFP, *n*=18 cells, *P*=0.049 *t*-test) and a significant increase in the fraction of fluorescent WPBs that underwent exocytosis (VWFpp–EGFP, black trace, 28.0±1.5%, 517 fusion events, *n*=30 cells; SYT5–EGFP, grey trace, 36.7±1.63%, 512 fusion events, *n*=18 cells, *P*<0.0004, *t*-test). Consistent with live imaging data, SYT5–mEGFP overexpression significantly increased histamine-evoked VWFpp secretion (Fig. 3B). No effect of SYT5 overexpression was found on WPB movements or on the fraction of WPBs showing restricted motion close to the plasma membrane (Fig. S3B), indicating that SYT5 does not contribute to WPB immobilisation at the plasma membrane.

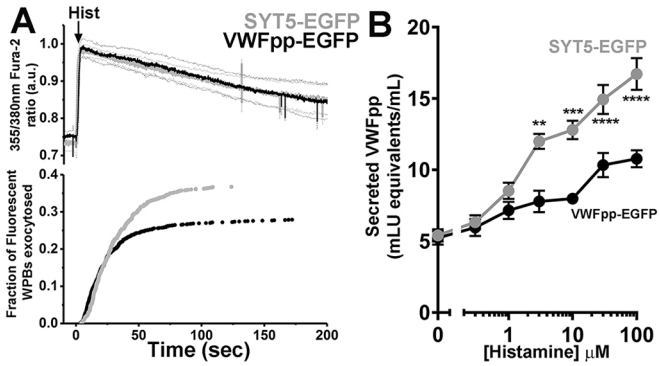

Fig. 3. SYT5 overexpression increases WPB exocytosis and VWFpp secretion. (A) The top panel shows the mean 355 nm/380 nm Fura-2 fluorescence ratio recorded in HUVECs expressing VWFpp–EGFP (black, *n*=12 cells) or SYT5–EGFP (grey, *n*=12 cells) together with VWFpp–EGFP and stimulated with histamine (100 µM, arrow). Thin dashed lines show the ±95% confidence limits for the mean fluorescence ratios. The lower panel shows cumulative plots of histamine-evoked WPB fusion times scaled to the mean fraction of WPBs that underwent exocytosis. (B) Histamine (0.3–100 µM)-evoked VWFpp secretion from HUVECs expressing VWFpp–EGFP (black) or SYT5–EGFP (grey) after lentiviral transduction. Data is mean±s.e.m of three independent experiments, each carried out in triplicate. **P*≤0.05, ***P*≤0.01, ****P*≤0.001, *****P*≤0.0001, *t*-test.

A Ca^{2+}-independent SYT5 mutant decreases histamine-evoked WPB exocytosis

To confirm that SYT5 function depends on its ability to sense Ca^{2+}, we mutated the third aspartate residue of the Ca^{2+}-binding motif of the C2A domain of SYT5–mEGFP to a serine to generate the Ca^{2+}-insensitive mutant SYT5-Asp197Ser–mEGFP (von Poser et al., 1997) (Fig. 4A) and overexpressed this in HUVECs via Nucleofection™. SYT5-Asp197Ser–mEGFP localised to WPBs [Fig. 4B; Manders' colocalisation coefficients M1 and M2 of 0.993±0.0007 and 0.920±0.013, respectively (*n*=10 cells)]. Analysis of WPB exocytosis revealed a dominant-negative effect of SYT5-Asp197Ser–mEGFP on a background of WT SYT5. SYT5-Asp197Ser–mEGFP significantly reduced both the mean maximal rate of WPB exocytosis from 3.1±0.53 WPBs/second (VWFpp–EGFP; *n*=17) to 1.4±0.29 WPBs/second (SYT5-Asp197Ser–mEGFP, *n*=25 cells) (*P*=0.0046, *t*-test) and the fraction of fluorescent WPBs that underwent exocytosis (VWFpp-EGFP, black trace, 38.9±3.5%, 532 fusion events, *n*=17 cells; SYT5-Asp197Ser-mEGFP, grey trace, 23.1±1.5%, 422 fusion events, *n*=27 cells, *P*<0.0001, *t*-test) (Fig. 4C).

Our results provide evidence for a role for SYT5 in regulating Ca^{2+}-dependent WPB exocytosis. SYT5 was the first non-neuronal member of the SYT family to be described (Hudson and Birnbaum, 1995, Craxton and Geodert, 1995) and has been implicated in regulating Ca^{2+}-driven exocytosis in neuronal, endocrine and neuroendocrine cell types (Birch et al., 1992; Fukuda et al., 2002; Gut et al., 2001; Iezzi et al., 2004; Lynch and Martin, 2007; Roper

Journal of Cell Science (2019) 132, jcs221952. doi:10.1242/jcs.221952

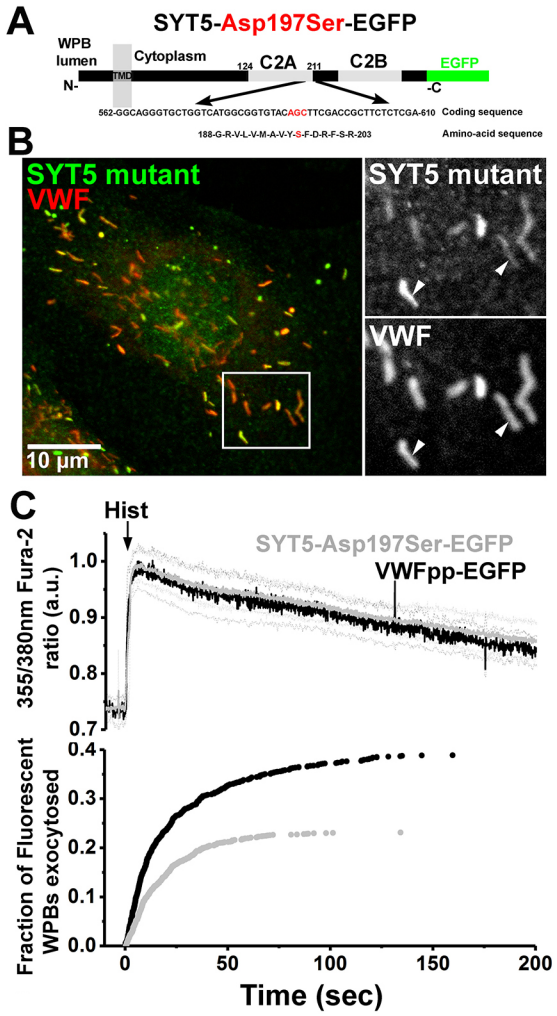

Fig. 4. Ca^{2+}-independent SYT5 mutant decreases WPB exocytosis. (A) Cartoon showing the point mutation, Asp197Ser, in the C2A domain of SYT5–EGFP generating the Ca^{2+}-insensitive mutant. (B) Fluorescence image of a HUVEC expressing SYT5-Asp197Ser–EGFP (48 h post-transfection) and immunolabelled for GFP (green; rabbit antibody) and endogenous VWF (red, sheep antibody). Arrowheads in grayscale images show the localisation of SYT5-Asp197Ser—EGFP to WPBs. Manders' colocalisation coefficients for the fractional overlap of EGFP signal with that of the WPB–VWF signal (Manders' coefficient M1) were 0.993±0.0007, and for WPB–VWF signal overlapping the EGFP signal (Manders' coefficient M2) 0.920±0.013 (n=10 cells). (C) The top panel shows the mean 355 nm/380 nm Fura-2 fluorescence ratio recorded in HUVECs expressing VWFpp–EGFP (black, n=12 cells) or SYT5-Asp197Ser–EGFP (grey, n=12 cells) stimulated with histamine (100 µM, arrow). Thin dashed lines show the ±95% confidence limits for the mean fluorescence ratios. The lower panel shows the cumulative plot of histamine-evoked WPB fusion times scaled to the mean fraction of WPBs that underwent exocytosis.

et al., 2015; Saegusa et al., 2002; Xu et al., 2007) as well as pH regulation of phagosomes and phagocytosis in macrophages (Vinet et al., 2008, 2009). SYT5 has a lower Ca^{2+}-affinity for phospholipid or SNARE protein interactions compared to the other main SYT reported to function in endocrine and neuroendocrine cell types, SYT7 (Chieregatti et al., 2004; Gustavsson et al., 2009; Hui et al., 2005; Iezzi et al., 2004; Schonn et al., 2008; Sugita et al., 2001). The higher Ca^{2+}-affinity of SYT7 is thought to underlie its role in asynchronous neurotransmitter release at low $[Ca^{2+}]_i$ (Bacaj et al., 2013; Luo and Sudhof, 2017; Weber et al., 2014), the sensitivity of SYT7-containing dense core vesicles of chromaffin cells to low $[Ca^{2+}]_i$ and weak stimulation (Rao et al., 2017), and in vesicle replenishment and release during insulin secretion as $[Ca^{2+}]_i$ declines to low levels (Dolai et al., 2016). However, the ability to sense low $[Ca^{2+}]_i$ during weak stimulation is not a prominent feature of endothelial WPBs. The rate of WPB exocytosis under resting conditions is very low (Erent et al., 2007) and WPB exocytosis is largely insensitive to small increases in $[Ca^{2+}]_i$ during weak stimulation (Birch et al., 1994; Erent et al., 2007). Studies in permeabilised or whole-cell patch-clamped endothelial cells show a supra micromolar $[Ca^{2+}]$ threshold for activation of WPB exocytosis (Frearson et al., 1995; Zupančič et al., 2002), and a requirement for sustained high (5–30 µM) $[Ca^{2+}]_i$ to drive strong exocytosis and VWF secretion (Birch et al., 1994, 1992; Carter and Ogden, 1994). Such high $[Ca^{2+}]_i$ are achieved during stimulation with physiological agonists or cell injury, such as occurs at wound sites (Carter and Ogden, 1994; Zupančič et al., 2002). SYT5 with its lower Ca^{2+}-affinity for phospholipid and SNARE protein interactions may help to limit WPB exocytosis during weak cell activation. This is potentially important because WPBs store high molecular mass forms of VWF that are potent at capturing platelets to the vessel wall, a process vital during primary haemostasis at wound sites (Sadler, 1998), but potentially hazardous if released inappropriately. Elevated VWF is a risk factor for coronary heart disease, ischaemic stroke and sudden death (van Schie et al., 2011; Wieberdink et al., 2010). WPBs also contain and co-release inflammatory mediators (P-selectin and chemokines) and tissue growth regulators (IGFBP7, Ang2) many of which have been linked to the aetiology of vascular disease (Papadopoulou et al., 2008). Thus, the involvement of a lower affinity SYT and a requirement for larger prolonged increases in $[Ca^{2+}]_i$ may minimise the risk of unwanted WPB exocytosis under normal conditions where endothelial cells may experience intermittent low level activation.

The nature of the molecular interactions between SYT5 and WPB SNAREs remain to be determined. Endothelial cells utilise at least two distinct SNARE complexes to regulate WPB exocytosis, one comprising syntaxin-4–SNAP23–VAMP3 and a second complex comprising syntaxin-3–SNAP23–VAMP8 (Fu et al., 2005; Matsushita et al., 2003; Schillemans et al., 2018b; van Breevoort et al., 2014; Zhu et al., 2015; Zhu et al., 2014), and each complex may play a role in specific modes of WPB exocytosis (Schillemans et al., 2018b). SYT–SNARE interactions have been extensively studied for neuronal SYT1, which binds both the neuronal SNAP (SNAP25) and syntaxin (syntaxin 1) in heterodimers or fully assembled SNARE complexes (reviewed in Chapman, 2008). SYT5 binds poorly to the WPB SNAP, SNAP23 (Chieregatti et al., 2004), and although the SYT5 C2AB domains can bind syntaxin 1 (Li et al., 1995) it remains to be established whether endothelial syntaxins implicated in WPB exocytosis bind SYT5. WPB exocytosis and VWFpp secretion was significantly reduced but not abolished upon depletion of endogenous SYT5. This is most likely due to the incomplete (~65%) depletion of SYT5 in these experiments, but may also reflect the involvement of other SYT isoforms in the Ca^{2+}-sensing mechanism and/or of the cytosolic Ca^{2+}-sensors CaM and the AnxA2–S100A10 complex described in the introduction. AnxA2-phospholipid interactions are typically low affinity and fit well with a general requirement for high $[Ca^{2+}]_i$ for WPB exocytosis. The ability of S100A10 to bind WPB-associated Munc13-4 (Chehab et al., 2017) and of AnxA2 to bind SNAP23 (Wang et al., 2007) indicate that WPB exocytosis is likely coordinated by a complex network of Ca^{2+}-sensors ensuring that WPB exocytosis only occurs when needed.

MATERIALS AND METHODS

Tissue culture, VWF and VWFpp ELISA assays, antibodies and reagents

Primary HUVECs tested for contamination were purchased from PromoCell GmbH (Heidelberg, Germany) and cultured as previously described (Hannah et al., 2005). Human embryonic kidney-293 (HEK-293) cells were cultured in Minimal Essential Medium (MEM) Alpha Medium 1× (Invitrogen) supplemented with 10% fetal calf serum (Biosera, Ringmer, UK) and 50 µg/ml gentamycin (Invitrogen) at 37°C, 5% CO_2 as previously described (Kiskin et al., 2010). Secreted VWF propolypeptide (VWFpp) was assayed by specific ELISA as previously described (Hewlett et al., 2011). Primary antibodies (Abs) along with the dilutions for immunofluorescence or western blotting are given in Table S1. All reagents were from Sigma-Aldrich unless otherwise stated. Fura-2/AM was from Invitrogen.

DNA constructs, site-directed mutagenesis, lentiviral production and transfection

The VWF propeptide fused to enhanced green fluorescent protein (VWFpp–EGFP) has been described previously (Hannah et al., 2005). A mEGFP fusion protein of human SYT5 (UniProtKB accession number O00445) was made by using the ligation-independent cloning (LIC) approach as previously described (Bierings et al., 2012) using the primers in Table S2. SYT1–EGFP was constructed by amplification of SYT1 from HUVEC cDNA using SYT1-specific primers that are flanked by HindIII target sequences (forward: 5′-AGT TT**AAGCTT**ATGGTGAGCGA-3′; HindIII site in bold) and AgeI sites (reverse; 5′-TAAA**ACCGGT**CCCT TCTTGACGGC-3′; AgeI site in bold), respectively. The 1289 bp amplicon was digested with HindIII and AgeI and was cloned in frame with EGFP between the HindIII and AgeI sites in EGFP-N1 (BD Biosciences Clontech, Saint-Germain-en-Laye, France). pSYT5-mCherry was made by transferring mCherry as an NheI/AgeI fragment from mCherry-N1 LIC vector (Bierings et al., 2012) to NheI/AgeI-digested SYT5–mEGFP. To make a shSYT5 resistant SYT5–mCherry construct, we used site-directed mutagenesis on pSYT5-mCherry to generate seven silent mutations along the shRNA target site (G518A, T521C, C524T, A527C, C530T, G533A, G536A). The genetic changes were introduced using Agilent's QuikChange II site-directed mutagenesis kit, forward primer 5′-AGGAAGTGAAGGGGCTGGGCCAAAGCTATATCGATAAAGTACA-GCCAGAAGTAGAGGAGCTGG-3′ and reverse primer 5′-CCAGCTCC-TCTACTTCTGGCTGTACTTTATCGATATAGCTTTGGCCCAGCCCC-TTCACTTCCT-3′. Correct integration of the desired mutations were confirmed using a CMV promoter targeting primer (5′-CAACGGG-ACTTTCCAAAATG-3′) and Sanger sequencing (Source Bioscience Ltd). The SYT5 Ca^{2+}-insensitive mutant (SYT5-Asp197Ser–EGFP) with the aspartate residue at position 197 (third aspartate in the Ca^{2+}-binding motif of the C2A domain) mutated to a serine residue (von Poser et al., 1997) was made by site-directed mutagenesis with the QuickChange® method (Agilent Technologies UK Limited, Cheshire, UK) using primers 5′-GGTCATGGCGGTGTAC**AGC**TTCGACCGCTTCTCT-3′ (forward) and 5′-AGAGAAGCGGTCGAA**GCT**GTACACCGCCATGACC-3′ (reverse) (mutated bases in bold). SYT5–mEGFP was transferred to a lentiviral vector by cloning a 2304 bp NdeI/AscI fragment or a 2598 bp NdeI/NotI fragment, respectively, into NdeI/AscI or NdeI/NotI digested LVX-mEGFP-LIC (van Breevoort et al., 2014).

SYT5 shRNA was obtained from the MISSION® shRNA library developed by The RNAi Consortium (TRC) at the Broad Institute of MIT and Harvard and distributed by Sigma-Aldrich (Table S3). Lentiviral vectors for transfection of SYT5-specific shRNA or mEGFP-tagged SYT5 constructs were made as follows. LKO.1-puro-CMV-TagRFP-U6-shC002 (Sigma), a puromycin-selectable lentiviral vector expressing MISSION® library shRNAs from the U6 promoter and TagRFP from the CMV promoter, was cut with NheI and PstI to replace TagRFP with a NheI-SalI-BclI-FseI-XmaI-PacI-PstI linker formed by annealing oligonucleotides RBNL204 (5′-CTAGCGTCGACTGATCAGGCCGGCCCCCGGGTTA-ATTAACTGCA-3′) and RBNL205 (5′-GTTAATTAACCCGGGGGC-CGGCCTGATCAGTCGACG-3′), yielding LKO.1-puro-CMV-linker-U6-shC002. LKO.1-puro-CMV-mEGFP-U6-shC002, which simultaneously expresses mEGFP and shRNAs from the CMV and U6 promoter respectively, was constructed by amplifying mEGFP from mEGFP-LIC (Bierings et al., 2012) with RBNL232 (5′-TATATGAT-CACTATGGTGAGCAAGGGCGAGGAGCTGTTC-3′) and RBNL222 (5′- ATATGGCCG GCCTTACTTGTACAGCTCGTCCATGCCG-3′). The 744 bp amplicon was digested with BclI and FseI, and cloned between the BclI and FseI sites in LKO.1-puro-CMV-linker-U6-shC002. LKO.1-puro-CMV-VWFpp-mEGFP-U6-shC002, fluorescently labelling WPBs through expression of VWFpp–mEGFP and simultaneously knocking down target SYT using shRNA from the MISSION® library, was constructed by amplifying VWFpp–EGFP (Hannah et al., 2005) with RBNL214 (5′- TATAGCTAGCGCCACCATGATTCCTGCCAGATTTG-CCGGGG-3′) and RBNL222. The 3058 bp amplicon was digested with NheI and FseI, and cloned between the NheI and FseI sites in LKO.1-puro-CMV-linker-U6-shC002. Clone TRCN0000000959 targeting SYT5 had lost the EcoRI site. Primers were designed to amplify the shRNA cassette flanked by a 5′ SphI and a 3′ EcoRI site (forward: 5′-TCGT-**GCATGC**CGATTG GTGGAAGTAAGG-3′, SphI restriction site in bold; reverse: 5′-GCCT**GAATTC**AAAAACCAGAGTT ACATAGACAAG-GTC-3′, EcoRI restriction site in bold). The 2064 bp amplicon was digested with SphI and EcoRI, and cloned between SphI- and EcoRI-sites in LKO.1-puro-CMV-mEGFP and LKO.1-puro-CMV-VWFpp-mEGFP vectors. The constructs were sequence verified. Lentiviral plasmids were produced in Stbl3 bacteria.

Lentiviral transduction and transfection via Nucleofection

Lentiviral production in HEK293T cells and lentiviral transductions of HUVECs were performed essentially as described previously (van Breevoort et al., 2014). pMD2-G (Addgene plasmid #12259), pRSV-Rev (Addgene plasmid #12253) and pMDLg/pRRE (Addgene plasmid #12251) helper plasmids were deposited by Didier Trono (Dull et al., 1998). Lentivirally transduced endothelial cells were selected using puromycin treatment (0.5 µg/ml for 48 h). After 48 h incubation, transduced HUVECs were passaged in six-well plates, 24-well plates or 35 mm poly-D-lysine-coated glass bottom culture dishes (MatTeK, Ashland, MA) depending on the experiment conditions. ELISA, quantitative PCR (qPCR), western blotting or live-cell imaging were performed on the transduced HUVECs when confluent. For conventional transfection of HUVECs, the Amaxa Nucleofection™ system was used with HUVEC OLD Nucleofector™ Solution containing 2–4 µg of target DNA and programme U-01, according to the manufacturer's instructions (Lonza Biologics, Slough, UK). Cells were used for experiments 48 h following transfection. HEK cell transfection via Nucleofection™ was identical to that for HUVECs with the exceptions that MEM Alpha medium was used in place of human growth medium (HGM), Cell Line Nucleofector™ Solution V was used in place of HUVEC OLD Nucleofector™ Solution, and the Nucleofection programme was Q-01.

RT-PCR and qPCR analysis

RNA was extracted using an RNeasy Mini Kit (QIAGEN). The quantity and purity of extracted RNA was determined by measuring its absorbance at 280 and 260 nm using a Nandrop-1000® device (ThermoFisher Scientific, Denmark). cDNA was synthesised using the High-Capacity cDNA Reverse Transcription Kit (Applied Biosystems, ThermoFisher Scientific). Briefly, 1 µg of RNA was added to the reaction mix, and cDNA was synthesised using one cycle of heating to 55°C for 20 min following by an increase to 94°C for 2 min. Subsequent PCR amplification of HUVEC cDNA was achieved using 40 cycles of denaturation (94°C for 15 s), followed by annealing (55°C for 30 s) and extension (72°C for 1 min). PCR was performed using a Mastercycler® machine (Eppendorf, Stevenage, UK). The products of PCR were run on a 1.5% agarose gel and visualised by ethidium bromide staining. All bands were sequenced verified (GATC Biotech, Cologne, Germany).

Immunocytochemistry and immunoblotting

For immunocytochemistry, HUVECs or HEK cells were grown on 9 mm glass coverslips and immunostaining and confocal fluorescence imaging of fixed cells were performed as previously described (Blagoveshchenskaya et al., 2002). For intensity measurements, exposures at each wavelength were first set to ensure that there was no detector saturation on the brightest

sample and then kept constant for all images. Images were prepared in Adobe Photoshop CS6. Immunoblotting was carried out as previously described (Bierings et al., 2012).

Live-cell imaging, vesicle tracking, confocal imaging of fixed cells and fluorescence overlap analysis

Exocytosis of VWFpp–EGFP-containing and EGFP–SYT5-associated WPBs were determined as previously described (Erent et al., 2007; Knipe et al., 2010). The moment of fusion of EGFP–SYT5-containing WPBs was determined by visualising the abrupt decrease in WPB fluorescence that occurs on fusion, as previously described (Knipe et al., 2010). Automatic tracking of WPB movements was carried out as previously described (Conte et al., 2016). Image data were acquired at 10 frames/second in Winfluor (http://spider.science.strath.ac.uk/sipbs/software_imaging.htm), exported as raw format to GMimPro/Motility freeware software (Dr Gregory Mashanov, Francis Crick Institute Mill Hill Laboratory, London; www.mashanov.uk). The automatic single particle tracking (ASPT) module in GMimPro (Mashanov and Molloy, 2007) was used to track the *x*,*y* position in time of individual WPBs expressing VWFpp–EGFP or SYT5–EGFP, yielding maximum velocities and maximum displacements. ASPT settings were full width and half maximum (FWHM) of 500 nm, R7, L20, Q25 and C5000. The time, *x* and *y* positions for WPBs for individual cells were exported in text file format for subsequent analysis of mean squared displacement (MSD) in MATLAB using custom written functions (available from the corresponding author upon request). MSD plots were fitted as previously described and the proportion of WPBs showing subdiffusive/restricted diffusion and their corresponding cage radii were determined (Conte et al., 2016). Confocal images for fixed cells were taken at room temperature using either a Leica SP2 or SP8 confocal microscopes (Mannheim, Germany) equipped with 40×, 63× and 100× objectives (HCX PL APO40×1.2 NA, PLAPO 63×/1.40, PLAPO100×1.4NA) or a Bio-Rad Radiance 2100 confocal microscope running LaserSharp 2000 software and equipped with a Nikon 60× and ×100 PLAPO 1.40 NA objectives. Dual-color images were acquired sequentially with pinhole setting Airy 1, image size 1024×1024 and frame averaging over 6–12 scans. To determine the fractional overlap of green (EGFP) with red (VWF) signals (Manders' colocalisation coefficient M1) or vice versa (Manders' colocalisation coefficient M2) in images of HUVECs expressing SYT5–GFP or SYT5-Asp197Ser–mEGFP and stained for endogenous VWF, we used the ImageJ plugin JACoP that implements the Manders' colocalisation coefficient with the Costes method for automatically estimating threshold values for identifying background levels (Costes et al., 2004), as reviewed in (Dunn et al., 2011).

Statistical analysis

Data were plotted in Origin 2017 or GraphPad Prism Version 7.02. Statistical analysis was achieved by a nonparametric *t*-test (except where indicated) using GraphPad Prism Version 7.02. Significance values are shown on the figures or in figure legends. Data are shown as mean±s.e.m.

Acknowledgements

We would like to thank Dr John Dempster (University of Strathclyde, Strathclyde Institute of Pharmacy and Biomedical Sciences, Glasgow, G1 1XQ UK) for his continuing support and development of the Winfluor imaging software used in this study.

Competing interests

The authors declare no competing or financial interests.

Author contributions

Conceptualization: M.J.H., R.B., T.C.; Methodology: D.O., R.B, T.C.; Formal analysis: C.L., J.S., R.B., T.C.; Investigation: C.L., J.S., D.O., R.B., T.C.; Resources: M.J.H., R.B., T.C.; Writing - original draft: T.C.; Writing - review & editing: C.L., D.O., T.C.; Supervision: M.J.H., R.B., T.C.; Project administration: T.C.; Funding acquisition: T.C.

Funding

T.C. was supported by an UK Medical Research Council (MRC) (grant MC_PC_13053). C.L. was supported by an St George's University London PhD studentship. R.B. was supported by a European Hematology Association Research Fellowship and by a grant from the Landsteiner Foundation for Blood Transfusion Research (LSBR-1707).

Supplementary information

Supplementary information available online at
http://jcs.biologists.org/lookup/doi/10.1242/jcs.221952.supplemental

References

Babich, V., Meli, A., Knipe, L., Dempster, J. E., Skehel, P., Hannah, M. J. and Carter, T. (2008). Selective release of molecules from Weibel Palade bodies during a lingering kiss. *Blood* **111**, 5282-5290.

Bacaj, T., Wu, D., Yang, X., Morishita, W., Zhou, P., Xu, W., Malenka, R. C. and Südhof, T. C. (2013). Synaptotagmin-1 and synaptotagmin-7 trigger synchronous and asynchronous phases of neurotransmitter release. *Neuron* **80**, 947-959.

Bai, J., Wang, C.-T., Richards, D. A., Jackson, M. B. and Chapman, E. R. (2004). Fusion pore dynamics are regulated by synaptotagmin*t-SNARE interactions. *Neuron* **41**, 929-942.

Bierings, R., Hellen, N., Kiskin, N., Knipe, L., Fonseca, A.-V., Patel, B., Meli, A., Rose, M., Hannah, M. J. and Carter, T. (2012). The interplay between the Rab27A effectors Slp4-a and MyRIP controls hormone-evoked Weibel-Palade body exocytosis. *Blood* **120**, 2757-2767.

Birch, K. A., Pober, J. S., Zavoico, G. B., Means, A. R. and Ewenstein, B. M. (1992). Calcium/calmodulin transduces thrombin-stimulated secretion: studies in intact and minimally permeabilized human umbilical vein endothelial cells. *J. Cell Biol.* **118**, 1501-1510.

Birch, K. A., Ewenstein, B. M., Golan, D. E. and Pober, J. S. (1994). Prolonged peak elevations in cytoplasmic free calcium ions, derived from intracellular stores, correlate with the extent of thrombin-stimulated exocytosis in single human umbilical vein endothelial cells. *J. Cell. Physiol.* **160**, 545-554.

Blagoveshchenskaya, A. D., Hannah, M. J., Allen, S. and Cutler, D. F. (2002). Selective and signal-dependent recruitment of membrane proteins to secretory granules formed by heterologously expressed von Willebrand factor. *Mol. Biol. Cell* **13**, 1582-1593.

Brandherm, I., Disse, J., Zeuschner, D. and Gerke, V. (2013). cAMP-induced secretion of endothelial von Willebrand factor is regulated by a phosphorylation/dephosphorylation switch in annexin A2. *Blood* **122**, 1042-1051.

Carter, T. D. and Ogden, D. (1994). Acetylcholine-stimulated changes of membrane potential and intracellular Ca2+ concentration recorded in endothelial cells in situ in the isolated rat aorta. *Pflugers Arch.* **428**, 476-484.

Chapman, E. R. (2008). How does synaptotagmin trigger neurotransmitter release? *Annu. Rev. Biochem.* **77**, 615-641.

Chehab, T., Santos, N. C., Holthenrich, A., Koerdt, S. N., Disse, J., Schuberth, C., Nazmi, A. R., Neeft, M., Koch, H., Man, K. N. M. et al. (2017). A novel Munc13-4/S100A10/Annexin A2 complex promotes Weibel-Palade body exocytosis in endothelial cells. *Mol. Biol. Cell* **28**, 1688-1700.

Chieregatti, E., Chicka, M. C., Chapman, E. R. and Baldini, G. (2004). SNAP-23 functions in docking/fusion of granules at low Ca2+. *Mol. Biol. Cell* **15**, 1918-1930.

Conte, I. L., Cookson, E., Hellen, N., Bierings, R., Mashanov, G. and Carter, T. (2015). Is there more than one way to unpack a Weibel-Palade body? *Blood* **126**, 2165-2167.

Conte, I. L., Hellen, N., Bierings, R., Mashanov, G. I., Manneville, J. B., Kiskin, N. I., Hannah, M. J., Molloy, J. E. and Carter, T. (2016). Interaction between MyRIP and the actin cytoskeleton regulates Weibel-Palade body trafficking and exocytosis. *J. Cell Sci.* **129**, 592-603.

Costes, S. V., Daelemans, D., Cho, E. H., Dobbin, Z., Pavlakis, G. and Lockett, S. (2004). Automatic and quantitative measurement of protein-protein colocalization in live cells. *Biophys. J.* **86**, 3993-4003.

Craxton, M. and Goedert, M. (1995). Synaptotagmin V: a novel synaptotagmin isoform expressed in rat brain. *FEBS Lett.* **361**, 196-200.

Craxton, M. (2010). A manual collection of Syt, Esyt, Rph3a, Rph3al, Doc2, and Dblc2 genes from 46 metazoan genomes–an open access resource for neuroscience and evolutionary biology. *BMC Genomics* **11**, 37.

Davis, A. F., Bai, J., Fasshauer, D., Wolowick, M. J., Lewis, J. L. and Chapman, E. R. (1999). Kinetics of synaptotagmin responses to Ca2+ and assembly with the core SNARE complex onto membranes. *Neuron* **24**, 363-376.

Disse, J., Vitale, N., Bader, M.-F. and Gerke, V. (2009). Phospholipase D1 is specifically required for regulated secretion of von Willebrand factor from endothelial cells. *Blood* **113**, 973-980.

Dolai, S., Xie, L., Zhu, D., Liang, T., Qin, T., Xie, H., Kang, Y., Chapman, E. R. and Gaisano, H. Y. (2016). Synaptotagmin-7 functions to replenish insulin granules for exocytosis in human islet β-cells. *Diabetes* **65**, 1962-1976.

Dull, T., Zufferey, R., Kelly, M., Mandel, R. J., Nguyen, M., Trono, D. and Naldini, L. (1998). A third-generation lentivirus vector with a conditional packaging system. *J. Virol.* **72**, 8463-8471.

Dunn, K. W., Kamocka, M. M. and McDonald, J. H. (2011). A practical guide to evaluating colocalization in biological microscopy. *Am. J. Physiol. Cell Physiol.* **300**, C723-C742.

Erent, M., Meli, A., Moisoi, N., Babich, V., Hannah, M. J., Skehel, P., Knipe, L., Zupančič, G., Ogden, D. and Carter, T. (2007). Rate, extent and concentration dependence of histamine-evoked Weibel-Palade body exocytosis determined from individual fusion events in human endothelial cells. *J. Physiol.* **583**, 195-212.

Frearson, J. A., Harrison, P., Scrutton, M. C. and Pearson, J. D. (1995). Differential regulation of von Willebrand factor exocytosis and prostacyclin synthesis in electropermeabilized endothelial cell monolayers. *Biochem. J.* **309**, 473-479.

Fu, J., Naren, A. P., Gao, X., Ahmmed, G. U. and Malik, A. B. (2005). Protease-activated receptor-1 activation of endothelial cells induces protein kinase Calpha-dependent phosphorylation of syntaxin 4 and Munc18c: role in signaling p-selectin expression. *J. Biol. Chem.* **280**, 3178-3184.

Fukuda, M., Kowalchyk, J. A., Zhang, X., Martin, T. F. J. and Mikoshiba, K. (2002). Synaptotagmin IX regulates Ca2+-dependent secretion in PC12 cells. *J. Biol. Chem.* **277**, 4601-4604.

Gerke, V. (2016). Annexins A2 and A8 in endothelial cell exocytosis and the control of vascular homeostasis. *Biol. Chem.* **397**, 995-1003.

Gustavsson, N., Wei, S.-H., Hoang, D. N., Lao, Y., Zhang, Q., Radda, G. K., Rorsman, P., Südhof, T. C. and Han, W. (2009). Synaptotagmin-7 is a principal Ca2+ sensor for Ca2+ -induced glucagon exocytosis in pancreas. *J. Physiol.* **587**, 1169-1178.

Gut, A., Kiraly, C. E., Fukuda, M., Mikoshiba, K., Wollheim, C. B. and Lang, J. (2001). Expression and localisation of synaptotagmin isoforms in endocrine (β)-cells: their function in insulin exocytosis. *J. Cell Sci.* **114**, 1709-1716.

Hamilton, K. K. and Sims, P. J. (1987). Changes in cytosolic Ca2+ associated with von Willebrand factor release in human endothelial cells exposed to histamine. Study of microcarrier cell monolayers using the fluorescent probe indo-1. *J. Clin. Invest.* **79**, 600-608.

Han, W., Rhee, J.-S., Maximov, A., Lao, Y., Mashimo, T., Rosenmund, C. and Südhof, T. C. (2004). N-glycosylation is essential for vesicular targeting of synaptotagmin 1. *Neuron* **41**, 85-99.

Hannah, M. J., Skehel, P., Erent, M., Knipe, L., Ogden, D. and Carter, T. (2005). Differential kinetics of cell surface loss of von Willebrand factor and its propolypeptide after secretion from Weibel-Palade bodies in living human endothelial cells. *J. Biol. Chem.* **280**, 22827-22830.

Hewlett, L., Zupančič, G., Mashanov, G., Knipe, L., Ogden, D., Hannah, M. J. and Carter, T. (2011). Temperature-dependence of weibel-palade body exocytosis and cell surface dispersal of von willebrand factor and its propolypeptide. *PLoS ONE* **6**, e27314.

Huang, J., Haberichter, S. L. and Sadler, J. E. (2012). The B subunits of Shiga-like toxins induce regulated VWF secretion in a phospholipase D1-dependent manner. *Blood* **120**, 1143-1149.

Hudson, A. W. and Birnbaum, M. J. (1995). Identification of a nonneuronal isoform of synaptotagmin. *Proc Natl Acad Sci USA* **92**, 5895-5899.

Hui, E., Bai, J., Wang, P., Sugimori, M., Llinas, R. R. and Chapman, E. R. (2005). Three distinct kinetic groupings of the synaptotagmin family: candidate sensors for rapid and delayed exocytosis. *Proc. Natl. Acad. Sci. USA* **102**, 5210-5214.

Iezzi, M., Kouri, G., Fukuda, M. and Wollheim, C. B. (2004). Synaptotagmin V and IX isoforms control Ca2+ -dependent insulin exocytosis. *J. Cell Sci.* **117**, 3119-3127.

Kang, R., Swayze, R., Lise, M. F., Gerrow, K., Mullard, A., Honer, W. G. and El-Husseini, A. (2004). Presynaptic trafficking of synaptotagmin I is regulated by protein palmitoylation. *J. Biol. Chem.* **279**, 50524-50536.

Kiskin, N. I., Hellen, N., Babich, V., Hewlett, L., Knipe, L., Hannah, M. J. and Carter, T. (2010). Protein mobilities and P-selectin storage in Weibel-Palade bodies. *J. Cell Sci.* **123**, 2964-2975.

Kiskin, N. I., Babich, V., Knipe, L., Hannah, M. J. and Carter, T. (2014). Differential cargo mobilisation within Weibel-Palade bodies after transient fusion with the plasma membrane. *PLoS ONE* **9**, e108093.

Knipe, L., Meli, A., Hewlett, L., Bierings, R., Dempster, J., Skehel, P., Hannah, M. J. and Carter, T. (2010). A revised model for the secretion of tPA and cytokines from cultured endothelial cells. *Blood* **116**, 2183-2191.

Li, C., Ullrich, B., Zhang, J. Z., Anderson, R. G. W., Brose, N. and Südhof, T. C. (1995). Ca2+-dependent and -independent activities of neural and non-neural synaptotagmins. *Nature* **375**, 594-599.

Lorenzi, O., Frieden, M., Villemin, P., Fournier, M., Foti, M. and Vischer, U. M. (2008). Protein kinase C-delta mediates von Willebrand factor secretion from endothelial cells in response to vascular endothelial growth factor (VEGF) but not histamine. *J. Thromb. Haemost.* **6**, 1962-1969.

Lowenstein, C. J., Morrell, C. N. and Yamakuchi, M. (2005). Regulation of Weibel-Palade body exocytosis. *Trends Cardiovasc. Med.* **15**, 302-308.

Luo, F. and Sudhof, T. C. (2017). Synaptotagmin-7-mediated asynchronous release boosts high-fidelity synchronous transmission at a central synapse. *Neuron* **94**, 826-839 e3.

Lynch, K. L. and Martin, T. F. J. (2007). Synaptotagmins I and IX function redundantly in regulated exocytosis but not endocytosis in PC12 cells. *J. Cell Sci.* **120**, 617-627.

Mashanov, G. I. and Molloy, J. E. (2007). Automatic detection of single fluorophores in live cells. *Biophys. J.* **92**, 2199-2211.

Matsushita, K., Morrell, C. N., Cambien, B., Yang, S.-X., Yamakuchi, M., Bao, C., Hara, M. R., Quick, R. A., Cao, W., O'Rourke, B. et al. (2003). Nitric oxide regulates exocytosis by S-nitrosylation of N-ethylmaleimide-sensitive factor. *Cell* **115**, 139-150.

Nightingale, T. D., White, I. J., Doyle, E. L., Turmaine, M., Harrison-Lavoie, K. J., Webb, K. F., Cramer, L. P. and Cutler, D. F. (2011). Actomyosin II contractility expels von Willebrand factor from Weibel-Palade bodies during exocytosis. *J. Cell Biol.* **194**, 613-629.

Nightingale, T. D., McCormack, J. J., Grimes, W., Robinson, C., Lopes da Silva, M., White, I. J., Vaughan, A., Cramer, L. P. and Cutler, D. F. (2018). Tuning the endothelial response: differential release of exocytic cargos from Weibel-Palade bodies. *J. Thromb. Haemost.* **16**, 1873-1886.

Pang, Z. P. and Südhof, T. C. (2010). Cell biology of Ca2+-triggered exocytosis. *Curr. Opin. Cell Biol.* **22**, 496-505.

Papadopoulou, C., Corrigall, V., Taylor, P. R. and Poston, R. N. (2008). The role of the chemokines MCP-1, GRO-alpha, IL-8 and their receptors in the adhesion of monocytic cells to human atherosclerotic plaques. *Cytokine* **43**, 181-186.

Rao, T. C., Santana Rodriguez, Z., Bradberry, M. M., Ranski, A. H., Dahl, P. J., Schmidtke, M. W., Jenkins, P. M., Axelrod, D., Chapman, E. R., Giovannucci, D. R. et al. (2017). Synaptotagmin isoforms confer distinct activation kinetics and dynamics to chromaffin cell granules. *J. Gen. Physiol.* **149**, 763-780.

Robinson, I. M., Ranjan, R. and Schwarz, T. L. (2002). Synaptotagmins I and IV promote transmitter release independently of Ca(2+) binding in the C(2)A domain. *Nature* **418**, 336-340.

Rondaij, M. G., Bierings, R., van Agtmaal, E. L., Gijzen, K. A., Sellink, E., Kragt, A., Ferguson, S. S. G., Mertens, K., Hannah, M. J., van Mourik, J. A. et al. (2008). Guanine exchange factor RalGDS mediates exocytosis of Weibel-Palade bodies from endothelial cells. *Blood* **112**, 56-63.

Roper, L. K., Briguglio, J. S., Evans, C. S., Jackson, M. B. and Chapman, E. R. (2015). Sex-specific regulation of follicle-stimulating hormone secretion by synaptotagmin 9. *Nat. Commun.* **6**, 8645.

Sadler, J. E. (1998). Biochemistry and genetics of von Willebrand factor. *Annu. Rev. Biochem.* **67**, 395-424.

Saegusa, C., Fukuda, M. and Mikoshiba, K. (2002). Synaptotagmin V is targeted to dense-core vesicles that undergo calcium-dependent exocytosis in PC12 cells. *J. Biol. Chem.* **277**, 24499-24505.

Schillemans, M., Karampini, E., Kat, M. and Bierings, R. (2018a). Exocytosis of Weibel-Palade bodies: how to unpack a vascular emergency kit. *J. Thromb. Haemost.* **17**, 6-18.

Schillemans, M., Karampini, E., van den Eshof, B., Gangaev, A., Hofman, M., van Breevoort, D., Meems, H., Janssen, H., Mulder, A. A., Jost, C. R. et al. (2018b). The Weibel-Palade body localized SNARE (Soluble NSF Attachment Protein Receptor) syntaxin-3 modulates von willebrand factor secretion from endothelial cells. *Arterioscler. Thromb. Vasc. Biol.* **38**, 1549-1561.

Schonn, J.-S., Maximov, A., Lao, Y., Sudhof, T. C. and Sorensen, J. B. (2008). Synaptotagmin-1 and -7 are functionally overlapping Ca2+ sensors for exocytosis in adrenal chromaffin cells. *Proc. Natl. Acad. Sci. USA* **105**, 3998-4003.

Südhof, T. C. (2014). The molecular machinery of neurotransmitter release (Nobel Lecture). *Angew. Chem. Int. Ed.* **53**, 12696-12717.

Sugita, S., Han, W., Butz, S., Liu, X., Fernandez-Chacon, R., Lao, Y. and Sudhof, T. C. (2001). Synaptotagmin VII as a plasma membrane Ca^{2+} sensor in exocytosis. *Neuron* **30**, 459-473.

Valentijn, K. M., Sadler, J. E., Valentijn, J. A., Voorberg, J. and Eikenboom, J. (2011). Functional architecture of Weibel-Palade bodies. *Blood* **117**, 5033-5043.

van Breevoort, D., van Agtmaal, E. L., Dragt, B. S., Gebbinck, J. K., Dienava-Verdoold, I., Kragt, A., Bierings, R., Horrevoets, A. J. G., Valentijn, K. M., Eikenboom, J. C. et al. (2012). Proteomic screen identifies IGFBP7 as a novel component of endothelial cell-specific Weibel-Palade bodies. *J. Proteome Res.* **11**, 2925-2936.

van Breevoort, D., Snijders, A. P., Hellen, N., Weckhuysen, S., van Hooren, K. W. E. M., Eikenboom, J., Valentijn, K., Fernandez-Borja, M., Ceulemans, B., De Jonghe, P. et al. (2014). STXBP1 promotes Weibel-Palade body exocytosis through its interaction with the Rab27A effector Slp4-a. *Blood* **123**, 3185-3194.

van Schie, M. C., de Maat, M. P., Isaacs, A., van Duijn, C. M., Deckers, J. W., Dippel, D. W. and Leebeek, F. W. (2011). Variation in the von Willebrand factor gene is associated with von Willebrand factor levels and with the risk for cardiovascular disease. *Blood* **117**, 1393-1399.

Vinet, A. F., Fukuda, M. and Descoteaux, A. (2008). The exocytosis regulator Synaptotagmin V controls phagocytosis in macrophages. *J. Immunol.* **181**, 5289-5295.

Vinet, A. F., Fukuda, M., Turco, S. J. and Descoteaux, A. (2009). The Leishmania donovani lipophosphoglycan excludes the vesicular proton-ATPase from phagosomes by impairing the recruitment of synaptotagmin V. *PLoS Pathog.* **5**, e1000628.

Vitale, N., Mawet, J., Camonis, J., Regazzi, R., Bader, M.-F. and Chasserot-Golaz, S. (2005). The Small GTPase RalA controls exocytosis of large dense core

secretory granules by interacting with ARF6-dependent phospholipase D1. *J. Biol. Chem.* **280**, 29921-29928.

von Poser, C., Ichtchenko, K., Shao, X., Rizo, J. and Sudhof, T. C. (1997). The evolutionary pressure to inactivate. A subclass of synaptotagmins with an amino acid substitution that abolishes Ca2+ binding. *J. Biol. Chem.* **272**, 14314-14319.

Wang, P., Chintagari, N. R., Gou, D., Su, L. and Liu, L. (2007). Physical and functional interactions of SNAP-23 with annexin A2. *Am. J. Respir. Cell Mol. Biol.* **37**, 467-476.

Weber, J. P., Toft-Bertelsen, T. L., Mohrmann, R., Delgado-Martinez, I. and Sørensen, J. B. (2014). Synaptotagmin-7 is an asynchronous calcium sensor for synaptic transmission in neurons expressing SNAP-23. *PLoS ONE* **9**, e114033.

Wieberdink, R. G., van Schie, M. C., Koudstaal, P. J., Hofman, A., Witteman, J. C. M., de Maat, M. P. M., Leebeek, F. W. G. and Breteler, M. M. B. (2010). High von Willebrand factor levels increase the risk of stroke: the Rotterdam study. *Stroke* **41**, 2151-2156.

Xu, J., Mashimo, T. and Südhof, T. C. (2007). Synaptotagmin-1, -2, and -9: Ca(2+) sensors for fast release that specify distinct presynaptic properties in subsets of neurons. *Neuron* **54**, 567-581.

Zhu, Q., Yamakuchi, M., Ture, S., de la Luz Garcia-Hernandez, M., Ko, K. A., Modjeski, K. L., LoMonaco, M. B., Johnson, A. D., O'Donnell, C. J., Takai, Y. et al. (2014). Syntaxin-binding protein STXBP5 inhibits endothelial exocytosis and promotes platelet secretion. *J. Clin. Invest.* **124**, 4503-4516.

Zhu, Q., Yamakuchi, M. and Lowenstein, C. J. (2015). SNAP23 regulates endothelial exocytosis of von Willebrand factor. *PLoS ONE* **10**, e0118737.

Zupančič, G., Ogden, D., Magnus, C. J., Wheeler-Jones, C. and Carter, T. D. (2002). Differential exocytosis from human endothelial cells evoked by high intracellular Ca(2+) concentration. *J. Physiol.* **544**, 741-755.

Supplementary Materials

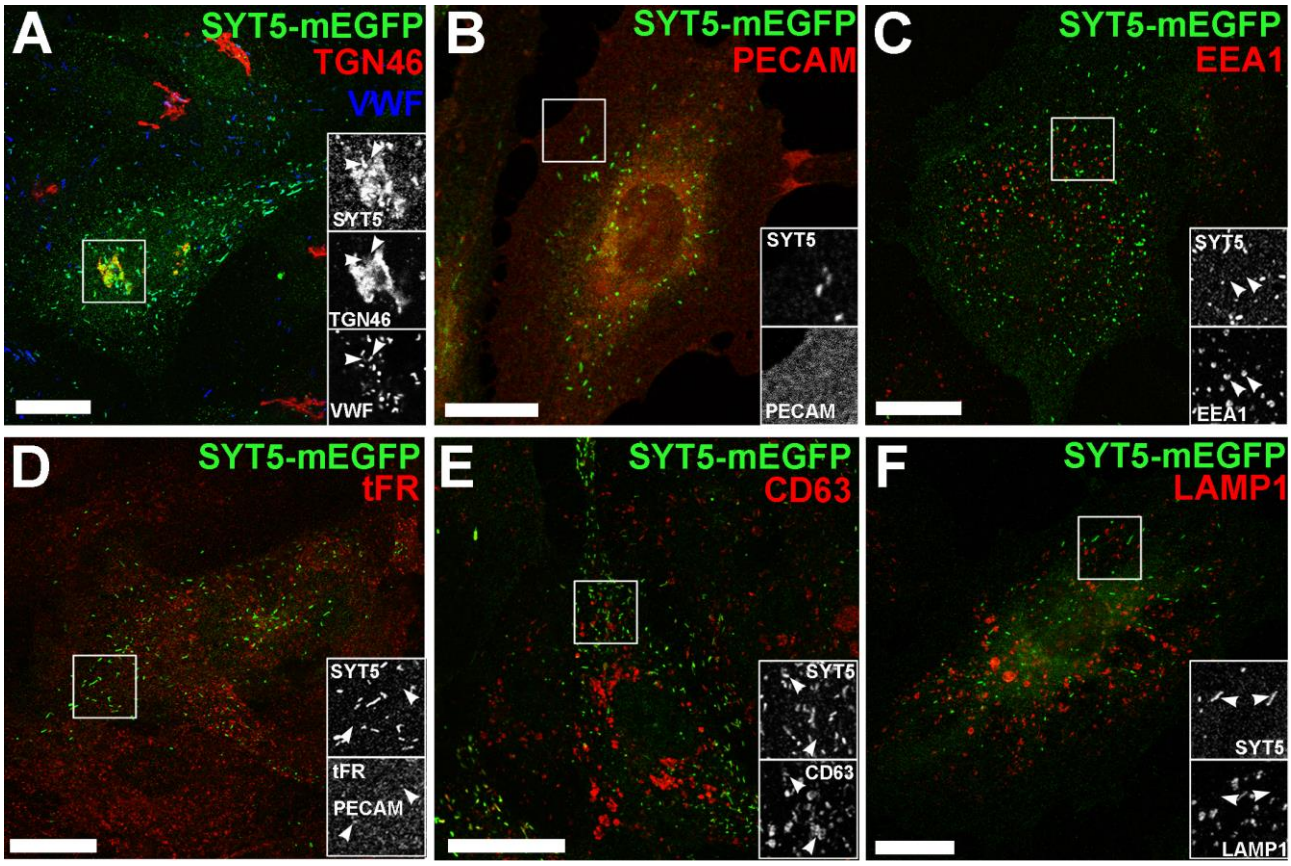

Figure S1. Subcellular distribution of SYT5-mEGFP. Confocal fluorescence images of single HUVEC 24 hours after Nucleofection™ with SYT5-mEGFP, and immuno-labeled with specific antibodies to GFP (sheep; green), VWF (top left panel only, rabbit; blue) and (A) TGN46, (B) PECAM, (C) tFR, (D) EEA1, (E) CD63 or (F) LAMP1 as indicated (red). Scale bars are 10μm. Inset panels show in greyscale regions indicated by white box.

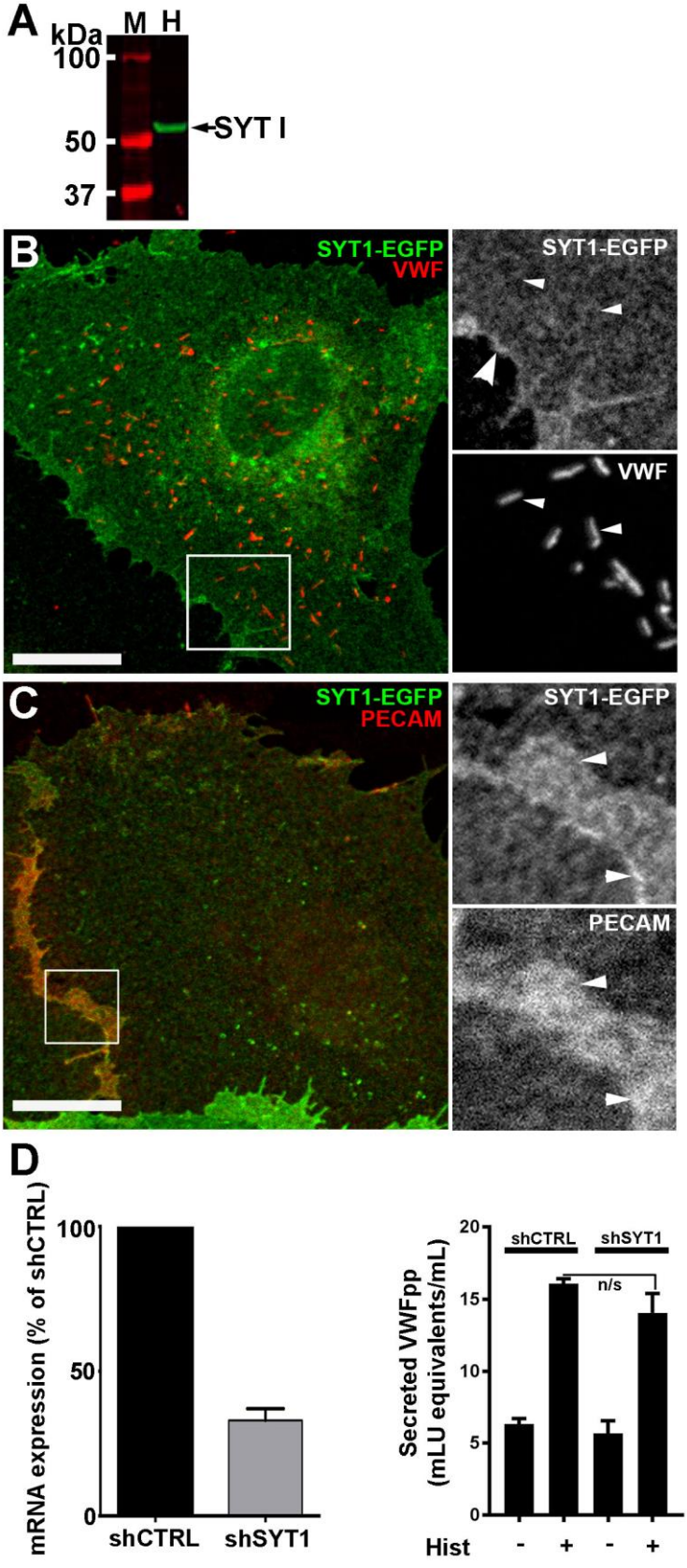

Figure S2 SYT1 is expressed in HUVEC but is not recruited to WPBs. (A) representative Western blot produced by probing HUVEC (H) lysate with the SYT1 primary antibody at a concentration of 1:200. The sizes of the marker (M) are shown on the left. A strong band at approximately 55 kDa represents SYT1 protein. (**B, C)**, Confocal fluorescence images of HUVEC 24 hours after Nucleofection™ with SYT1-mEGFP, and immuno-labeled with specific antibodies to (**B**) GFP (sheep; green), VWF (rabbit; red) and (**C**) GFP (sheep; green), PECAM (mouse; red) Scale bars are 10μm. Inset panels show in greyscale regions indicated by white box. (**D**) left; Quantification of shSYT1 mediated SYT1 mRNA depletion. Data is normalized to shCTRL and is mean±SEM of 3 independent experiments carried out in duplicate. Right; Histamine (100 μM) evoked VWFpp secretion in shCTRL or shSYT1 treated HUVEC. Experiment shown is mean ±sem and is representative of 3 independent experiments each carried out in triplicate.

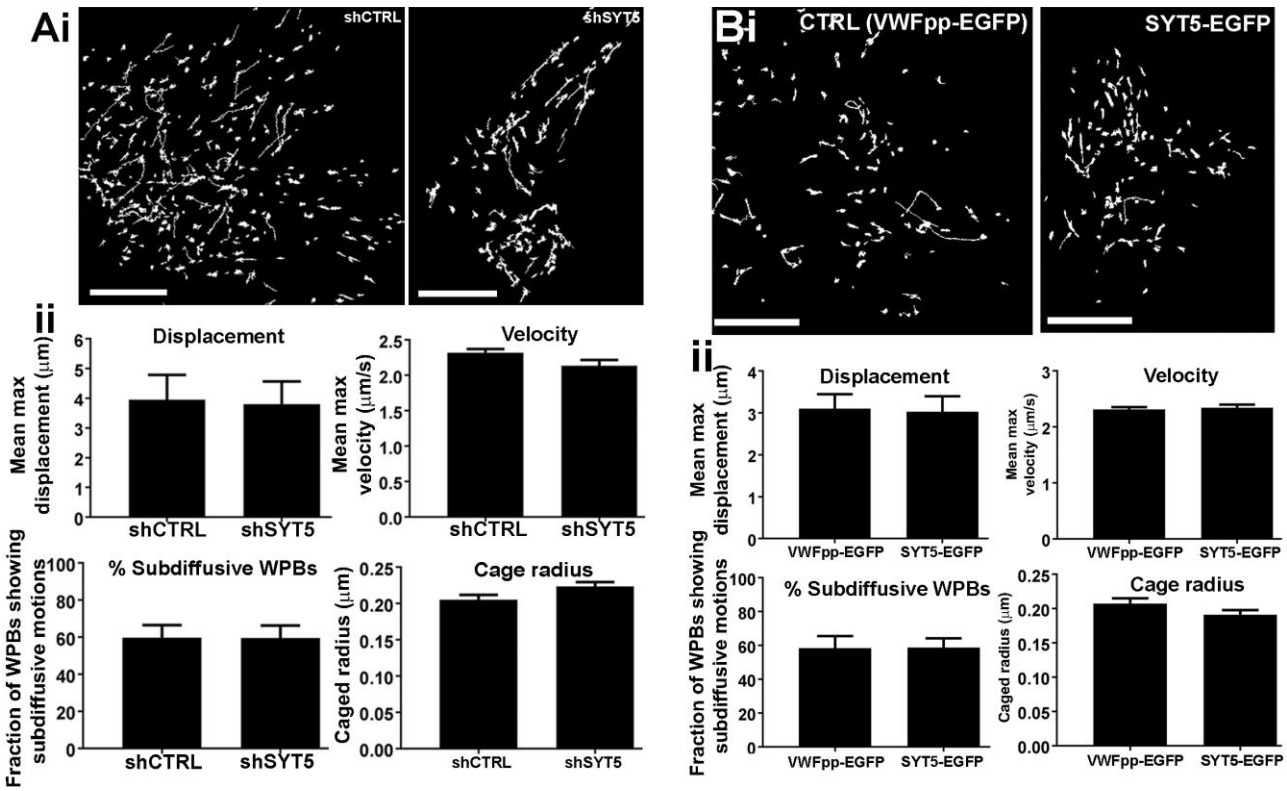

Figure S3. SYT5 depletion (A) or SYT5-EGFP overexpression (B) does not alter WPB trafficking close to the plasma membrane. (Ai). Representative X-Y trajectories of individual WPBs in single HUVEC expressing VWFpp-EGFP and following lentiviral transduction with shCTRL (**left**) or shSYT5 (**right**). Trajectories were determined here and elsewhere from TIRFM videos using the ASPT function of GMimPro software as described previously (Conte et al., 2016). Number of cells imaged and trajectories detected were: shCTRL, n=6 cells, 890 trajectories; shSYT5 n=6 cells, 740 trajectories. (**Aii).** Parameters determined from detected trajectories of long range (top panels) or short range (lower panels) WPB movements. Number of WPBs analysed for short range movements were: shCTRL, 135 trajectories; shSYT5, 149 trajectories. **(Bi).** Representative X-Y trajectories of individual WPBs in single HUVEC expressing VWFpp-EGFP (**i**) (control, n=7 cells, 693 trajectories) or SYT5-EGFP (**ii**) (n=7 cells, 735 trajectories) after lentiviral transduction. (**Aii).** Parameters determined from detected trajectories of long range (top panels) or short range (lower panels) WPB movements. Number of WPBs analysed for short range movements were: control, 76 trajectories; SYT5-EGFP, 103 trajectories.

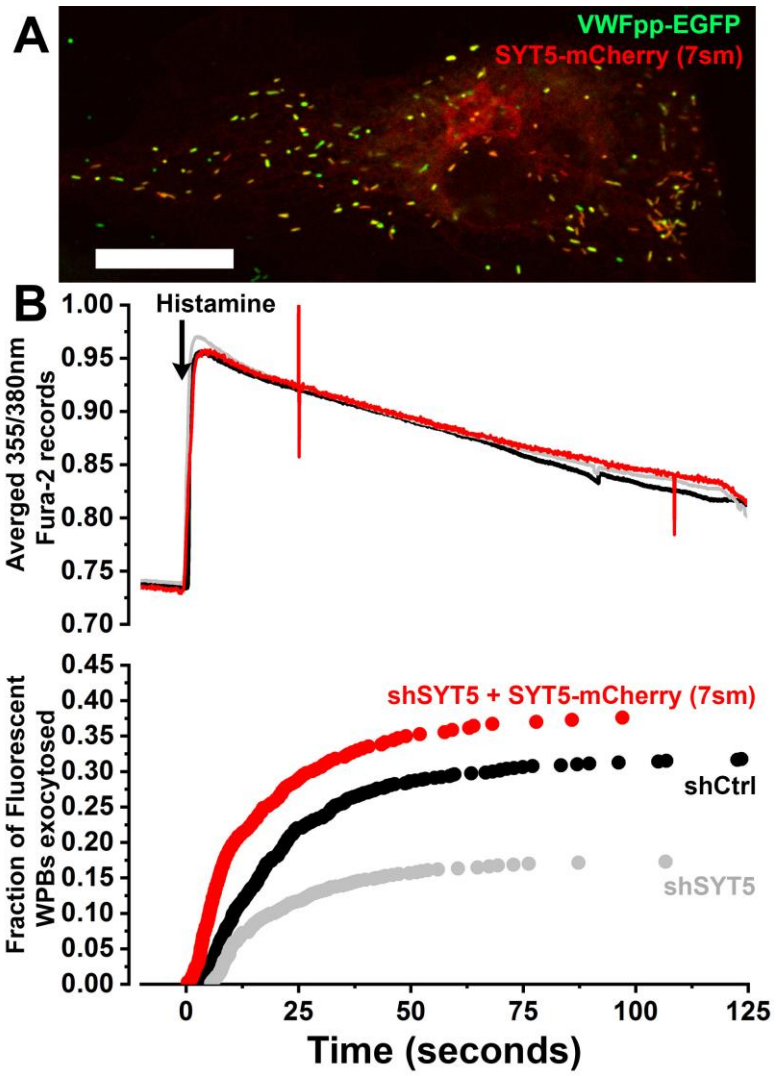

Figure S4. Overexpression of SYT5-mCherry (7sm) prevents shSYT5 mediated reduction in histamine-evoked WPB exocytosis in HUVEC. (A). Confocal fluorescence image of a HUVEC co-expressing VWFpp-EGFP (green) and SYT5-mCherry (7sm) (red) 24 hours post transfection. Scale bar is 10µm. (**B**) top panel shows averaged 355nm/380nm Fura-2 fluorescence ratios from shControl treated HUVEC (black, 10 cells), shSYT5 treated HUVEC (grey, 9 cells) and shSYT5 treated cells Nucleofected™ with SYT5-mCherry (7sm) (red, n=12 cells, 24 hrs post transfection). For clarity the ±95% confidence limits for the mean fluorescence ratios have been omitted. Histamine (100µM). Was added at the arrow. Lower panel in B shows cumulative plots of histamine-evoked WPB fusion times scaled by the mean fraction of WPBs that underwent exocytosis and colour coded as in (**A**). The mean (±SEM) maximal rates of WPB exocytosis in response to histamine were; shCtrl; 2.3 ± 0.3 WPBs/second, n=13 cells, shSYT5; 1.4 ± 0.2

WPBs/second, n=16 cells, and shSYT5 + SYT5-mCherry (7sm) 6.4 ± 1.1 WPBs/second, n=12 cells. The fraction of fluorescent WPBs that underwent exocytosis were; shCtrl; black trace 32.4 ± 1.4%, 136 fusion events, n=13 cells, shSYT5; grey trace,17.3 ± 2.9%, 129 fusion events, n=16 cells, and shSYT5 + SYT5-mCherry (7sm); red trace, 37.5 ± 3.1%, 158 fusion events, n=12 cells.

Supplementary Tables

Table S1. Antibody reagents.

Antigen	Manufacturer	Catalogue Number	Host Species	Optimum Dilution for ICC	Optimum Dilution for Western Blotting
VWF	DAKO	A0082	Rabbit	1:10000	N/A*
VWF	Serotec	AHP062	Sheep	1:10000	N/A
VWF	Serotec	MCA127	Mouse	1:100	N/A
Tubulin	Sigma-Aldrich	T9026	Mouse	N/A	1:5000
LAMP1	DSHB**	H4B4	Mouse	1:50	N/A
CD63	DSHB	H5C6	Mouse	1:200	N/A
EEA-1	BD Transduction Laboratories	610456/7	Mouse	1:100	N/A
TGN-46	Serotec	AHP500	Sheep	1:300	N/A
PDI	Stressgen	SPA-891	Mouse	1:500	N/A
tfR	Invitrogen	13-6800	Mouse	1:200	N/A
GFP	Molecular Probes	A-11122	Rabbit	1:300	Variable
GFP	Biogenesis	4745-1051	Sheep	1:250	Variable
GFP	Roche	11814460001	Mouse	1:500	N/A
PECAM	DSHB	PSB1	Mouse	1:10	N/A
SYT1	Synaptic Systems	105011	Mouse	1:200***	1:500
SYT5	Abcam®	ab116452	Rabbit	1:100	N/A
SYT 5	Abcam®	ab140432	Goat	N/D	1:300

Fluorophore- or horseradish peroxidase–coupled secondary Abs were from Jackson ImmunoResearch Europe (Newmarket, UK). Infrared dye secondary Ab were from LI-COR

Biosciences UK Ltd (Cambridge, UK). * N/A = Not Applicable. Western blotting or ICC was not performed for this antigen. ** DSHB = Developmental Studies Hybridoma Bank. *** Unless otherwise stated, the dilutions of the SYT antibodies for ICC were determined in HEK cells expressing fluorescent constructs of the SYT proteins.

Table S2. Primers sequence used for LIC.

SYT5	Forward Primer	Reverse Primer
	GCAGGGGCGCAACAGACCCCGGTATGTTCCCGGAGCCCCCAAC	CCACCAGGCCGGCCAGCACCCGGTCCGGGCGCAGGCAGCAGCCTCAC

Table S3. Synaptotagmin 5 shRNA used in this study

Synaptotagmin	shRNA clone MISSION® Library	shRNA target sequence
SYT5	TRCN0000000959	CCAGAGTTACATAGACAAGGT